ORIGINAL ARTICLE

A Robotic System with Robust Remote Center of Motion Constraint for Endometrial Regeneration Surgery

Jianhua Li[1,2,3], Chongyang Wang[1,2], Zhenxing Wang[1,2,3], Xiong Zheng[4], Zhidong Wang[5], Jichun Tan[6] and Hao Liu[1,2*]

Abstract

Surgical robots have been widely used in different procedures to improve and facilitate the surgery. However, there is no robot designed for endometrial regeneration surgery, which is a new therapy for restoring fertility in women using stem cells. Endometrial regeneration surgery requires processing of the endometrium and transplantation of stem cells with minimal trauma to the uterus. In this paper, we introduce a surgical robotic system that consists of a dexterous hysteroscope, supporting arm, and additional novel instruments to facilitate the operation and decrease trauma to the uterus. Remote center of motion (RCM) constraint is required to protect the cervix of the uterus. First, the supporting arm and hysteroscope are controlled separately in kinematics to ensure that the RCM constraint and hysteroscope's shape and posture are predictable. Then, a task-decoupled method is used to improve the robustness of the RCM constraint. Experiments confirm that the proposed method is more robust and achieves higher RCM accuracy. In addition, the master-slave control of a robot with RCM constraint is also verified. This study proposes the realization of a robot with robust RCM control for endometrial regeneration surgery.

Keywords: Endometrial regeneration, Surgical robot, Remote center of motion, Task decoupled
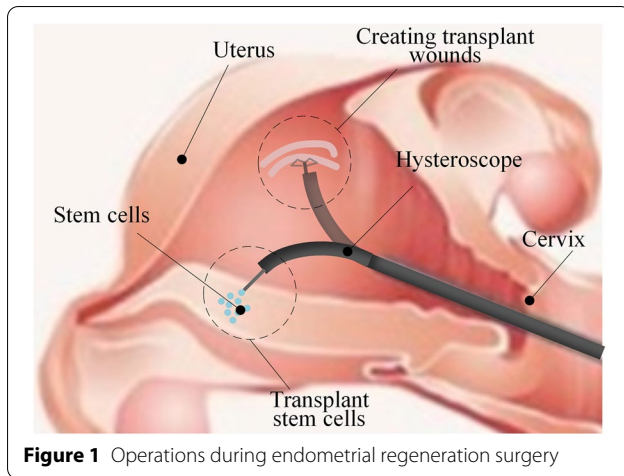
1 Introduction

According to data from the World Health Organization, the number of infertile women has increased to 30 million worldwide [1, 2]. Intrauterine adhesions (IUAs) are a major cause of secondary infertility; the majority of IUAs are associated with uterine damage due to intrauterine surgery [3, 4]. Traditional remedies such as the transcervical resection of adhesions and artificial hormone therapy have a high recurrence rate of IUAs. Stem cell therapy is a promising remedy to fundamentally cure endometrial damage [5–7]. Creating transplant wounds and transplanting stem cells are two key steps in endometrial regeneration surgery, as displayed in Figure 1.

However, handheld instruments and manual operation methods make surgery difficult and limit the efficacy of this new therapy. Moreover, these surgical procedures can cause secondary uterine damage. During endometrial regeneration surgery, a hysteroscope is inserted into the uterine cavity via the cervix. The motion of the hysteroscope is constrained by the cervix, which can be considered a remote center of motion (RCM) constraint. To facilitate this process and improve the outcome of stem cell therapy, a robot designed for endometrial regeneration surgery is required.

Several robotics systems have been designed by researchers for diverse surgeries [8–11]. The Da Vinci surgical system is the most successful commercial surgical robot. Although it has been used to perform a hysterectomy, surgery to remove a patient's uterus, it has no ability to process the endometrium without damaging the uterus [12]. Another surgical robot, the Hominis

*Correspondence: liuhao@sia.cn

[1] State Key Laboratory of Robotics, Shenyang Institute of Automation, Chinese Academy of Sciences, Shenyang 110016, China
Full list of author information is available at the end of the article

Li *et al. Chinese Journal of Mechanical Engineering*   (2022) 35:76

Page 2 of 13

Figure 1 Operations during endometrial regeneration surgery

surgical system, was designed for transvaginal surgical procedures at a single site [13]. It is also not applicable to endometrial regeneration surgery because its instruments work outside the uterus. Numerous robotic systems have been designed for natural orifice transluminal endoscopic surgery. He et al. proposed a robot-assisted method for nasal surgery [14]. Amanov et al. designed a surgical system using concentric tube robots to complete prostatectomy in the small luminal urethra space [15]. Similarly, Goldman et al. presented a continuum robot for transurethral surgery [16]. Bajo et al. introduced an endonasal telerobotic system for use in throat microsurgery [17]. Shang et al. designed a single-port robotic system for transcanal microsurgery [18]. Lau et al. design a flexible surgical robotic system for endoscopic submucosal dissection [19]. These robots have achieved significant progress in natural orifice transluminal surgery.

During endometrial regeneration surgery, the motion of the hysteroscope can suffer from RCM constraint. RCM constraint is a common problem in laparoscopic surgery and ophthalmic microsurgery [9, 20]. Mechanical RCM and programmable RCM are the two main methods for realizing RCM constraint during surgical manipulation. Addressing mechanical RCM, numerous researchers have proposed mechanical structures to realize RCM constraints. He et al. designed a novel RCM mechanism for a robot for retinal vascular bypass surgery [21]. Kim et al. proposed a novel gravity-compensation mechanism using RCM mechanisms [22]. Unlike mechanical RCM, programmable RCM is realized by software and is more flexible. To realize RCM constraint, two degree-of-freedom (DOFs) of the robot are required. Aghakhani et al. provided a general method to realize a surgical robot's control task with an RCM constraint using the kinematics of an extended task [23]. Similarly, Sadeghian et al. combined a task with an RCM constraint in an

RCM-constrained Jacobian [24]. However, the extended-task Jacobian could easily be singular. The tangent plane of the access port can also be used to express the kinematics of the RCM point [25]. However, determining the tangent plane is difficult during application. Sandoval et al. associated the RCM constraint with the task space using the minimum distance between the surgical tool and RCM point [26]. Using the null space of the robot provides another method to realize the RCM constraint [27–29]. A redundant robot is required to guarantee the RCM. Zhang and Li et al. realized the visual tracking control of an endoscope with RCM constraints [30, 31].

Examining the existing surgical robots, several of these can facilitate and improve different types of surgery; however, none are intended for endometrial regeneration surgery. In our previous work, a continuum manipulator was designed to reach targets in the endometrium [32]. For endometrial regeneration surgery, a robot is required to perform multiple tasks in the confined uterine cavity while ensuring the safety of the uterus. To protect the uterine cervix, the hysteroscope should be manipulated using an RCM constraint. In this study, we design a robotic system to facilitate and protect the uterus during endometrial regeneration surgery. To maintain flexibility while improving the stability of the robot, we propose a task-decoupled method to control the hysteroscope with robust RCM constraint. The method is evaluated by comparing it with a general method, the extended-task method. The control method of the robot is verified experimentally.

The remainder of this paper is organized as follows. Section 2 introduces the surgical procedure and design of the robotic system. Section 3 details the kinematics of the robot, realization of the RCM constraint, and control method of the robot. Section 4 presents the experiments and results. Section 5 concludes the study.

2 Design of the Robotic System
2.1 Surgical Procedure and Requirements
In endometrial regeneration surgery, the ultimate goal is to transplant stem cells into the uterus and regenerate the endometrium. To successfully perform endometrial regeneration surgery, tasks such as diagnosing the uterine cavity and processing the endometrium are required before stem cell transplantation. The procedure for endometrial regeneration surgery is as follows.

(1) Insert the hysteroscope into the vagina, through the cervix, and into the uterus.
(2) Observe the uterine cavity, locate the uterine horn, and determine the position of the transplantation.

(3) Insert the instrument used to create a wound through the channel of the hysteroscope into the uterine cavity. Manipulate the hysteroscope to locate the tip of the instrument at the position of the adhesions. Scratch the endometrium to remove the adhesions and create a regeneration environment for the stem cells.

(4) Replace the instrument used to create the wound with the transplant instrument. Transplant the stem cells on the transplant wounds.

To perform the operation in the uterine cavity, the hysteroscope must be small in size and high in dexterity. The small size of the hysteroscope can decrease the risk of cervical invasion. The high dexterity enables the hysteroscope to avoid pulling the cervix during the operation. The actual instruments must be sufficiently small to pass through the hysteroscope channel. The instrument to create the wound must be capable of scratching the endometrium with high quality and efficiency.

2.2 Design of Dexterous Hysteroscope

Hysteroscope is a key component of this surgical system. It feeds back a view of the uterine cavity and provides channels for the other instruments. Traditional rigid hysteroscopes are stiff and have low dexterity, which can damage the endometrium and cervix. More recent flexible diagnostic hysteroscopes have the advantages of smaller size and high compliance to ensure safety during diagnostics. However, these devices are not suitable for manipulation and suffer from poor load capabilities. To overcome these difficulties, we designed a hysteroscope with a flexible tip and rigid shaft body, as indicated in Figure 2. The hysteroscope provided an inner channel for the instruments used to function in the endometrium and transplant the stem cells. The diameter of the hysteroscope was 5 mm and the diameter of the inner channel was 2.5 mm. The length of the flexible segment was 30 mm. The flexible segment of the hysteroscope was driven by two cables and could realize planar deformation. The rigid segment of the hysteroscope was fixed to the actuation unit. The actuation unit had two lead screws that were used to pull the cables. To determine the pulling force, the two cables were separately fixed on two force sensors and the sensors were installed on the lead screws. In addition, a pair of gears was used to realize the rotation of the hysteroscope along the axis of the rigid segment. At the end of the actuation unit, there was a slot where an additional instrument could be inserted. The instrument could rotate along its axis by actuating the slot. To increase the dexterity of the hysteroscope, a supporting arm was used to provide additional DOFs to
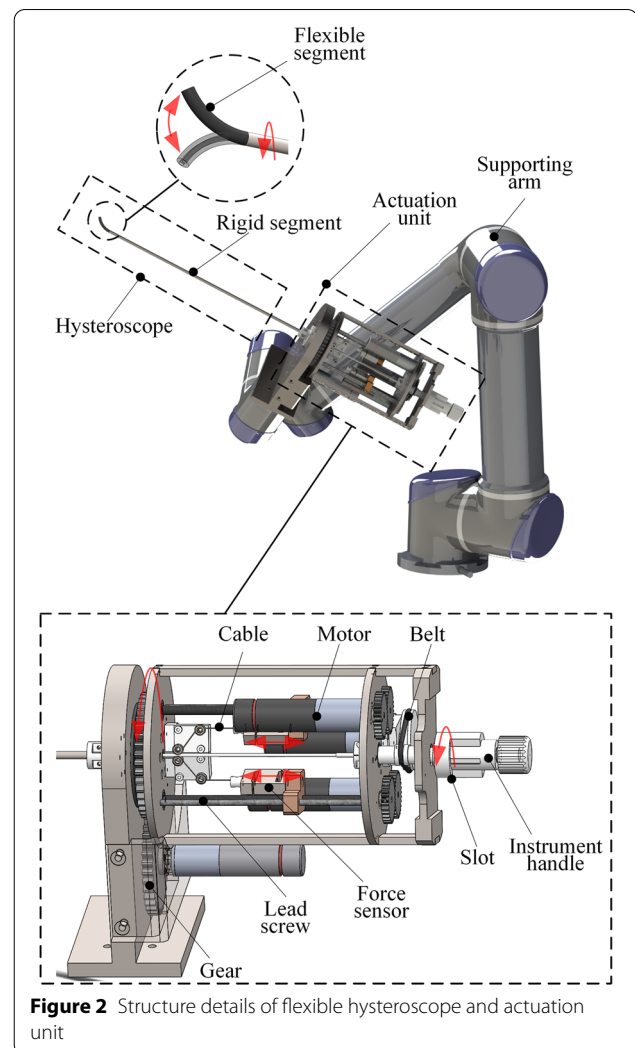

**Figure 2** Structure details of flexible hysteroscope and actuation unit

allow the hysteroscope to realize motions with the RCM constraint.

2.3 Design of Additional Instruments

Two types of instruments are used in endometrial regeneration surgery. One is an instrument used to scratch the endometrium. It was composed of a lantern-like slicer, sheath tube, and handle. The slicer had multiple thin beams that could be easily deformed. One end of the slicer was supported by a sheath tube. The other end of the slicer was fixed to the tip of a tendon that passed through the slicer and sheath. When pulling the tendon, the slicer could unfold, as displayed in Figure 3. The handle was used to control the folding and unfolding of the slicer. The handle was composed of two parts. One part was fixed with the sheath; the other part, similar to a nut, was fixed with the other tip of the tendon. By screwing

Figure 3 Design of instrument for scratching endometrium
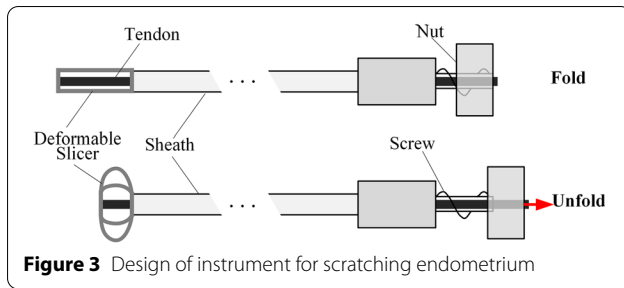
the nut, the tendon could be pulled or pushed, resulting in unfolding and folding of the slicer. The instrument used to scratch the endometrium is displayed in Figure 4. Figure 4(a) and (b) display an unfolded and folded slicer, respectively. In the folded and unfolded positions, the slicer maximum diameters were 1.5 mm and 6 mm, respectively. When the slicer was folded, it could pass through the channel in the hysteroscope. The handle was then inserted into the slot of the actuation unit. Figure 4(c) indicates the structure of the instrument at the proximal end. Figure 4(d) displays how the instrument is inserted into the slot of the actuation unit. When the slicer reaches the uterine cavity, it can be unfolded by screwing the nut. The deformed beam of the slicer then contacts the endometrial tissue. When actuating the slot, the slicer could be rotated to scratch the endometrium. The slicer was made of a thin-walled nitinol tube with an outer diameter (OD) of 1.27 mm and inner diameter (ID) of 1.07 mm. Thin beams were manufactured by grooving the tube using a laser cutting method. The width of the groove was 0.35 mm and the length of the groove was 6.5 mm; there were six grooves. The other instrument was a long tube used to transmit the stem cell suspension. The tube could also pass through the channel of the hysteroscope. The tube was connected to a syringe, which was used to control the injection volume of the stem cell suspension.

Figure 4 Instrument for scratching the endometrium

Figure 5 Overview of robotic system
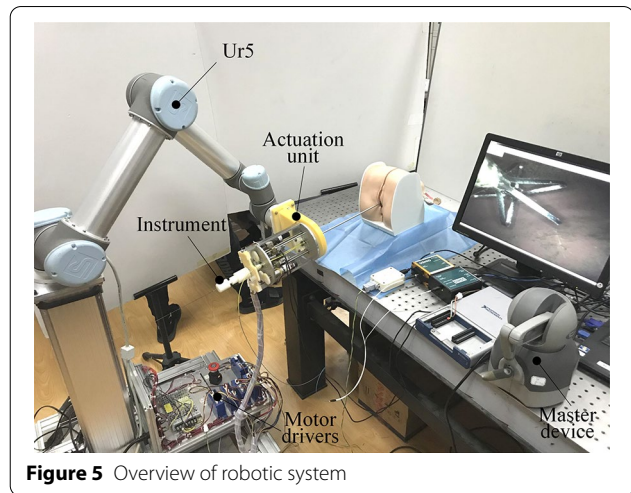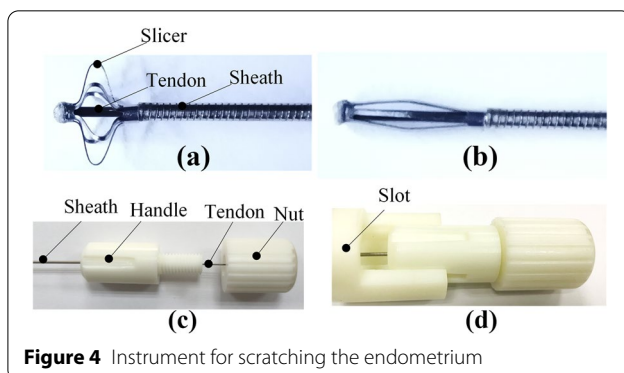
2.4 Integration of Robotic System

The robotic system used for endometrial regeneration surgery is displayed in Figure 5. It consists of a supporting arm, actuation unit, dexterous hysteroscope, and master device. The surgeon could view the uterine cavity on a monitor and control the motion of the hysteroscope by manipulating the master device. A UR5 arm was used to support the actuation unit and provide additional DOFs to control the motion of the hysteroscope with an RCM constraint. A camera with a resolution of 400×400 pixels was fixed to the hysteroscope to view the uterine cavity. The diameter of the camera was 1.7 mm. There were four motors in the actuation unit. Two of these were used to actuate the lead screws to pull the cables; one was used to actuate the gears to rotate the hysteroscope; the last was used to actuate the belt pulley to rotate the slicer. All motors were powered by drivers (Copley Driver, USA) and controlled by a controller (Copley CAN-USB; USA). In addition, two force sensors were used to provide feedback on the actuation force. The sensors were connected to two amplifiers (Futek; USA). Data acquisition equipment (NI DAQ; USA) was used to acquire the force data. Figure 6 displays the architecture of the robotic system.
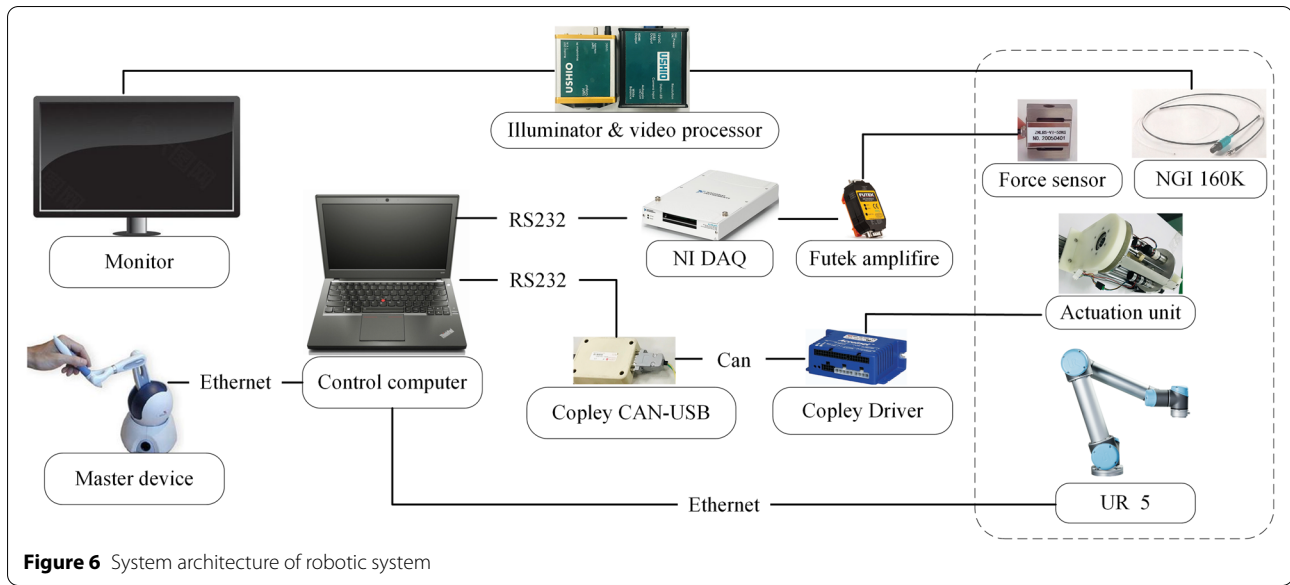
3 Methodology

In this section, we introduce the direct kinematics of the surgical robot and realization of the RCM constraint. Then, the control method for the complete surgical robot is introduced.

3.1 Kinematics of Surgical Robot

In the surgical system, the motion of the distal tip of the hysteroscope is related to the actuation and supporting arms. The actuation unit provides two DOFs: The rotation

Li *et al. Chinese Journal of Mechanical Engineering*   (2022) 35:76

Page 5 of 13

Figure 6 System architecture of robotic system

of the rigid segment and bending of the flexible segment. The UR5 arm supports the hysteroscope unit, provides the DOFs for remote center motion, and controls the position of the rigid segment of the hysteroscope. We define the joint vector of the UR5 arm as $\boldsymbol{q}_u = [\theta_1, \theta_2, ..., \theta_6]^{\mathrm{T}}$. The forward kinematics of the UR5 arm are expressed as

$$^0\boldsymbol{T}_u(\boldsymbol{q}_u) = \prod_{i=1}^{6} e^{\hat{\xi}_i\theta_i} \cdot {}^0\boldsymbol{M}_u, \tag{1}$$

where ξ_i is the screw axis of the ith joint and $^0\boldsymbol{M}_u$ is the transformation matrix from frame $\{u\}$ to frame $\{0\}$ when the joint values are zero, as indicated in Figure 7. For the actuation unit, the rotation angle of the rigid segment and bending angle of the flexible segment are defined separately as θ_7 and θ_8. Then, the transformation matrix of the hysteroscope tip is expressed as

$$^0\boldsymbol{T}_e = {}^0\boldsymbol{T}_u \cdot e^{\hat{\xi}_7\theta_7} \cdot {}^u\boldsymbol{M}_{s1} \cdot e^{\hat{\xi}_8L}, \tag{2}$$
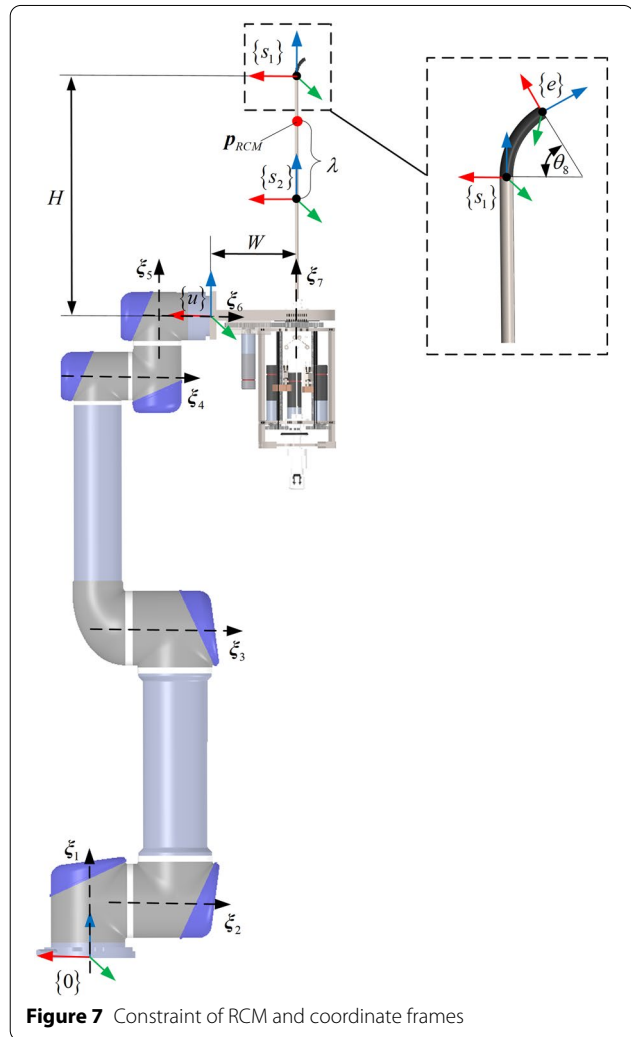
where ξ_7 and ξ_8 are the screw axes of the two additional joints, $\{s_1\}$ is the frame related to the tip of the rigid segment, $^u\boldsymbol{M}_{s1}$ is the transformation matrix from frame $\{s_1\}$ to frame $\{0\}$ when $\theta_7 = 0$, and L is the length of the flexible segment. ξ_7 has the format

$$\xi_7 = [0, W, 0, 0, 0, 1]^{\mathrm{T}}, \tag{3}$$

and ξ_8 has the format

$$\xi_8 = \left[0, 0, 1, 0, \frac{\theta_8}{L}, 0\right]^{\mathrm{T}}. \tag{4}$$

$^u\boldsymbol{M}_{s1}$ has the format

Figure 7 Constraint of RCM and coordinate frames

$$
^{u}M_{s1} = \begin{bmatrix} 1 & 0 & 0 & -W \\ 0 & 1 & 0 & 0 \\ 0 & 0 & 1 & H \\ 0 & 0 & 0 & 1 \end{bmatrix}, \tag{5}
$$

where H and W are the distances between frame $\{s_1\}$ and frame $\{u\}$ in x- and z-axis directions, respectively, as indicated in Figure 7. Hence, the direct kinematics of the robot are expressed.

3.2 RCM Constraint

During endometrial regeneration surgery, the hysteroscope passes through the cervix to reach the uterine cavity. The motion of the rigid segment is constrained by the cervix, which is considered the RCM constraint. To express the point on the rigid segment that instantaneously coincides with the position of the cervix, a variable related to the insertion depth is used [23]. As indicated in Figure 7, the RCM point on the rigid segment is expressed as

$$
\begin{aligned}
& \boldsymbol{p}_{RCM} = \boldsymbol{p}_{s2} + \lambda(\boldsymbol{p}_{s1} - \boldsymbol{p}_{s2}), \\
& 0 \le \lambda \le 1,
\end{aligned} \tag{6}
$$

where $\boldsymbol{p}_{s1}$ expresses the position of the distal tip of the rigid segment, $\boldsymbol{p}_{s2}$ is the position of another fixed point on the rigid segment, and λ is the parameter that indicates the insertion degree. For the two fixed points on the rigid segment, their Jacobians are expressed as

$$
\begin{aligned}
& \boldsymbol{J}_{s1} = Ad_{T_1}(\boldsymbol{J}_u^s), \\
& \boldsymbol{J}_{s2} = Ad_{T_2}(\boldsymbol{J}_u^s),
\end{aligned} \tag{7}
$$

where $\boldsymbol{J}_u^s$ is the spatial Jacobian of the UR5 arm, and $\boldsymbol{T}_1$ and $\boldsymbol{T}_2$ are two homogeneous matrices separately related to $\boldsymbol{p}_{s1}$ and $\boldsymbol{p}_{s2}$. The two homogeneous matrices have the following formats:

$$
\begin{aligned}
& \boldsymbol{T}_1 = \begin{bmatrix} \boldsymbol{I}_{3\times3} & \boldsymbol{p}_{s1} \\ 0 & 1 \end{bmatrix}, \\
& \boldsymbol{T}_2 = \begin{bmatrix} \boldsymbol{I}_{3\times3} & \boldsymbol{p}_{s2} \\ 0 & 1 \end{bmatrix}.
\end{aligned} \tag{8}
$$

Based on Eq. (6), the differential format of the RCM point is derived as

$$
\dot{\boldsymbol{p}}_{RCM} = \begin{bmatrix} \boldsymbol{J}_{s1,v} + \lambda(\boldsymbol{J}_{s2,v} - \boldsymbol{J}_{s1,v}) \\ \boldsymbol{p}_{s2} - \boldsymbol{p}_{s1} \end{bmatrix}^{\mathrm{T}} \begin{pmatrix} \dot{\boldsymbol{q}}_u \\ \dot{\lambda} \end{pmatrix}, \tag{9}
$$

where $\boldsymbol{J}_{s1,v}$ and $\boldsymbol{J}_{s2,v}$ are separately the translational part of the of $\boldsymbol{J}_{s1}$ and $\boldsymbol{J}_{s2}$.

For the supporting arm, two tasks are required: Tracking the desired position of the rigid segment tip and
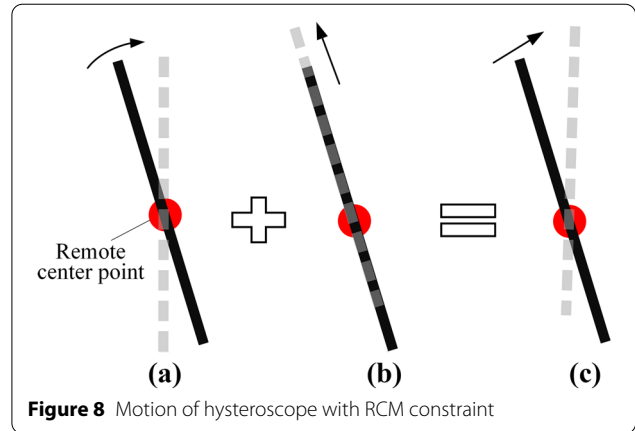

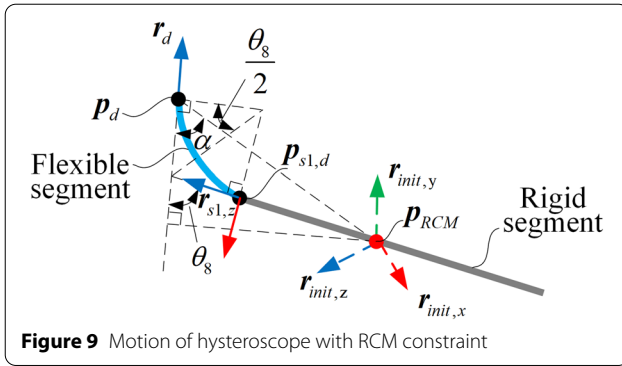**Figure 8** Motion of hysteroscope with RCM constraint

ensuring that the RCM point coincides with the cervical position. First, the error of the RCM is defined as

$$
\boldsymbol{e}_{RCM} = \boldsymbol{p}_c - \boldsymbol{p}_{RCM}, \tag{10}
$$

where $\boldsymbol{p}_c$ is the desired position of the remote center, i.e., the position of the cervix. Unlike the work of [23], which combines the two tasks into an extended task, we propose a task-decoupled method to realize robust RCM constraint. In the proposed method, the RCM constraint is considered as the primary task, where position tracking is achieved using the null space projector of the Jacobian of the RCM. This method does not increase the dimension of the Jacobian algorithm; therefore, algorithm singularity can be avoided. In addition, the error of the RCM can be maintained at a low level because the RCM constraint is the primary task in the algorithm. However, position tracking could fail if its position-tracking instantaneous motion conflicts with the RCM constraint. To ensure that the position-tracking task does not conflict with the RCM constraint task, the position-tracking instantaneous motion is decoupled into insertion and directional motions, as displayed in Figure 8. Figure 8(a) indicates the pure directional motion. Figure 8(b) is the pure insertion motion. Figure 8(c) displays the hybrid motion of the directional and insertion motions. For the RCM constraint, neither the insertion nor rotation motion can cause an error in the RCM. Thus, the joint velocity of the supporting arm is expressed as

$$
\dot{\boldsymbol{q}}_u = \boldsymbol{J}_{RCM}^{\#} \boldsymbol{e}_{RCM} + \left(\boldsymbol{I} - \boldsymbol{J}_{RCM}^{\#} \cdot \boldsymbol{J}_{RCM}\right) \begin{bmatrix} \dot{\boldsymbol{q}}_r & \dot{\lambda} \end{bmatrix}^{\mathrm{T}}. \tag{11}
$$

where $\boldsymbol{J}_{RCM}^{\#} = \boldsymbol{J}_{RCM}^{\mathrm{T}} \left(\boldsymbol{J}_{RCM} \cdot \boldsymbol{J}_{RCM}^{\mathrm{T}}\right)^{-1}$ is the pseudoinverse of the RCM Jacobian, $\dot{\boldsymbol{q}}_r$ is related to the directional motion, and $\dot{\lambda}$ is related to the insertion motion. To obtain the value $\dot{\boldsymbol{q}}_r$, which is used to realize directional

Figure 9 Motion of hysteroscope with RCM constraint

motion, the direction error must be defined. For the rigid segment, its desired direction $r_{s1,z}$ can be easily obtained using the desired position and position of the cervix. The desired direction of the rigid segment can be written as

$$r_{s1,z} = (p_{s1,d} - p_c)/|p_{s1,d} - p_c|, \qquad (12)$$

where $p_{s1,d}$ is the desired position of the rigid segment tip. Subsequently, the direction error of the rigid segment is expressed as

$$f_e(q_u) = r_{s1,z}^{\mathrm{T}} \cdot (p_{s1} - p_{s2})/|p_{s1} - p_{s2}|. \qquad (13)$$

Using the gradient of the direction error, $\dot{q}_r$ is obtained as

$$\dot{q}_r = k_e \cdot \nabla f_e/|\nabla f_e|, \qquad (14)$$

where k_e is a positive coefficient and ∇f_e is the gradient of the direction error. For the insertion motion, λ is written as

$$\dot{\lambda} = k_\lambda(\lambda_d - \lambda), \qquad (15)$$

where k_λ is a positive coefficient and λ_d is the desired insertion distance. Using Eq. (11), we can realize reliable control of the position tracking of the rigid segment with a remote center motion constraint.

3.3 Control of Robot System
During the surgical process, to reach the desired position and direction, both the supporting arm and flexible segment of the hysteroscope must be controlled.

Although the control of the entire robot system can be realized using the inverse differential kinematics of the robot system, the bending angle of the flexible segment is unpredictable during the iterative process. We directly calculate the bending and rotation angles of the flexible segment using the inverse kinematics of the

flexible segment. This ensures that the bending of the flexible segment is predicted. Therefore, the flexible segment and supporting arm are controlled separately in the kinematics, as indicated in Figure 9. First, we identify the desired position of the RCM point in the robotic frame. After engaging the teaching mode of the supporting arm, the tip of the hysteroscope can be moved to the desired position. Using the feedback values of the joints and initial value of λ, we can obtain the initial value of p_{RCM} and initial direction of the rigid segment $[r_{init,x}\ r_{init,y}\ r_{init,z}]$. The flexible segment is assumed to have a constant curvature. The relationship between the bending angle of the flexible segment θ_8 and target is indicated in Figure 8. We use the parameter α to determine whether bending is required for the flexible segment to reach the desired direction. It is defined as

$$\alpha = \arccos\left(r_d^{\mathrm{T}} \cdot \frac{(p_d - p_{RCM})}{|p_d - p_{RCM}|}\right), \qquad (16)$$

where p_d is the desired position and r_d is the desired direction. When $\alpha = 0$, no bending is required for the flexible segment. Under this condition, we have

$$\begin{aligned}
\theta_7 &= 0, \\
\theta_8 &= 0, \\
r_{s1,z} &= r_d, \\
p_{s1} &= p_d - L \cdot r_d.
\end{aligned} \qquad (17)$$

We considered the conditions for $\alpha \neq 0$. According to Figure 9, we can obtain θ_8 by solving

$$\left(|p_d - p_{RCM}|\cos\alpha - \frac{|p_d - p_{RCM}|\sin\alpha}{\tan\theta_8}\right)\frac{\theta_8}{\tan(\theta_8/2)} = L, \qquad (18)$$
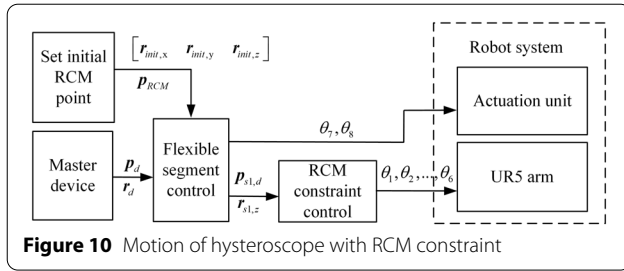
where L denotes the length of the flexible segment. Next, we obtain the desired direction of the rigid segment using

$$r_{s1,z} = \frac{p_d - \frac{L}{\theta_8}\tan\left(\frac{\theta_8}{2}\right)r_d - p_{RCM}}{\left|p_d - \frac{L}{\theta_8}\tan\left(\frac{\theta_8}{2}\right)r_d - p_{RCM}\right|}. \qquad (19)$$

The desired position of the rigid segment tip is expressed as

$$p_{s1,d} = p_d - \frac{L}{\theta_8}\tan\left(\frac{\theta_8}{2}\right)r_d - \frac{L}{\theta_8}\tan\left(\frac{\theta_8}{2}\right)r_{s1,z}. \qquad (20)$$

In addition, rotation of the segment is also required to bring the bending plane of the flexible segment parallel to the desired direction. The rotation angle θ_7 can be obtained using

Li *et al. Chinese Journal of Mechanical Engineering*   (2022) 35:76

Page 8 of 13

Figure 10 Motion of hysteroscope with RCM constraint

$$\theta_7 = \arccos\left(\left(\boldsymbol{r}_d \times \frac{(\boldsymbol{p}_d - \boldsymbol{p}_{RCM})}{|\boldsymbol{p}_d - \boldsymbol{p}_{RCM}|}\right)^{\mathrm{T}} \cdot \hat{\omega}_{s1} \cdot \boldsymbol{r}_{init,y}\right),$$
(21)

where $\hat{\omega}_{s1}$ is the skew-symmetry of the rotation vector in the direction of the rigid segment from $\boldsymbol{r}_{init,z}$ to $\boldsymbol{r}_{s1,z}$. It has the format

$$\boldsymbol{\omega}_{s1} = \boldsymbol{r}_{init,z} \times \boldsymbol{r}_{s1,z}.$$
(22)

Hence, the angles related to the flexible segment are all resolved. To control the supporting arm, $\boldsymbol{r}_{s1,z}$ and $\boldsymbol{p}_{s1,d}$ are used as inputs for the RCM control. A diagram of the control method for the robotic system is displayed in Figure 10.

4 Experiments

4.1 Parameters Identification of Flexible Segment

The desired bending angle of the flexible segment was calculated using its inverse kinematics. This was achieved by controlling the actuation displacements of the cables. To improve the control accuracy of the hysteroscope, parameters including the composite bending stiffness of the flexible segment and elastic coefficient of the cables must be identified. The bending stiffness of the hysteroscope differs when different instruments are in the channel. Therefore, three cases must be considered: no instrument in the channel, the slicer in the channel, and the tube in the channel. Figure 11(a) displays these three
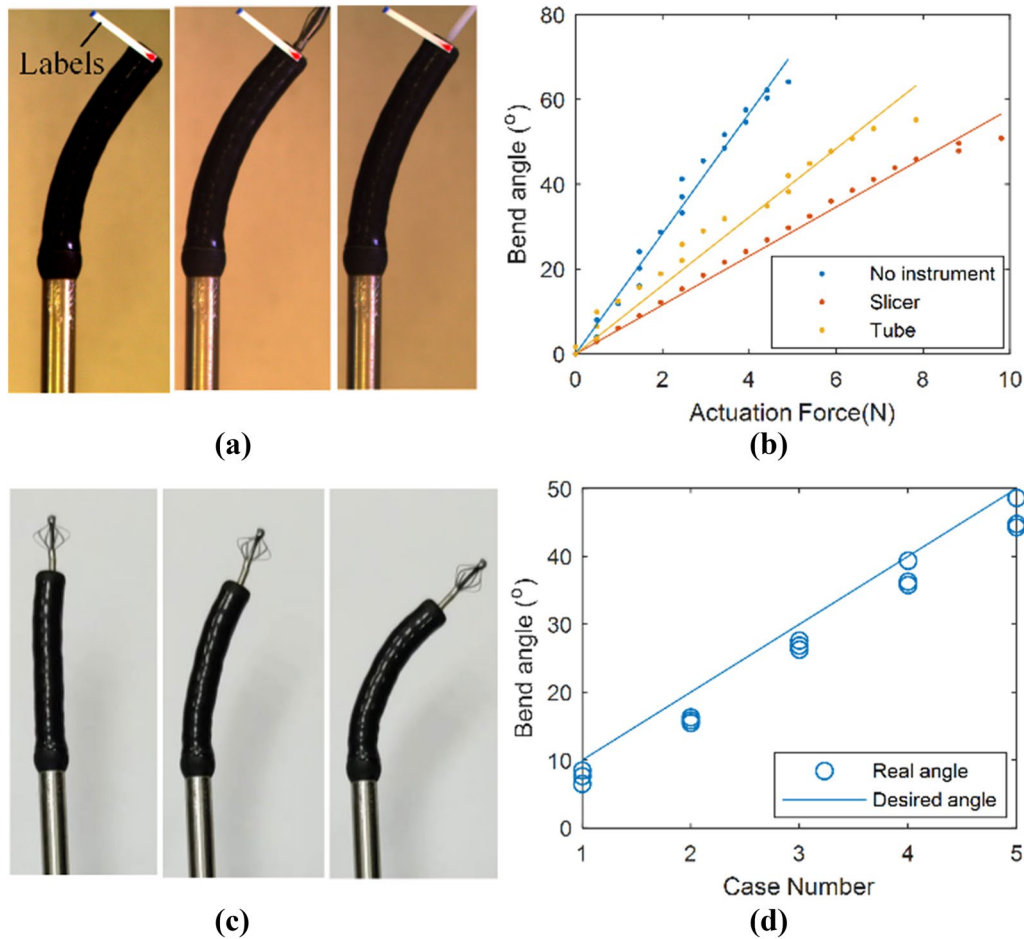
Figure 11 Evaluation of flexible segment

Table 1 Reach target with random initial joint values

Method	Success rate	Mean number of iterations	Mean e_{RCM}
Extended task	52/200	87	3.86
Task decoupled	141/200	153	0.68

cases. The flexible segment was deformed separately in each situation by pulling the cables. The actuation force and displacement were recorded during the processes. To determine the bend angle of the flexible segment, a colored label was attached to the tip of the flexible segment. The flexible segment was then captured by a camera and its bending angle was obtained using the method in Ref. [33]. Figure 11(b) indicates the relationship between the actuation force and bend angle for the different instruments in the hysteroscope. The bending stiffnesses of the three cases were 14.18, 5.77, and 8.06°/N. When the slicer was in the channel, the flexible segment demonstrated the greatest stiffness. The elastic coefficient of the cables was 0.076 mm/N. The elastic elongation of the cables can be compensated using these parameters. Experiments were performed to evaluate the bending angle accuracy of the flexible segment. Five desired bending angles varying from 10° to 50° at intervals of 10° were selected. The real bending angle of the flexible segment was measured using the images. The results are presented in Figure 11(d). The mean error was 3.3°. Figure 11(c) displays the moments of the slicer rotating when the flexible segment was bent. The rotational speed of the slicer was 200 r/min. The rotation of the slicer did not influence the robot system.

4.2 RCM Constraint Evaluation in Simulation

In this section, we compare the task-decoupled method (proposed method) with the general extended-task method using simulation. All control algorithms were written in MATLAB. In the simulation, the robustness and accuracy of the two methods for the RCM constraint were verified. First, the supporting arm was controlled to reach a target with a constant relative position of [10, 0, 30$^\mathrm{T}$ to the initial position. Two hundred random joint values within the range $[-\pi, \pi]$ were used as the initial joint values. The initial value of λ was set to 0.8. Algorithmic singularities or joint limits can be encountered during the process of reaching a desired position. Therefore, not all initial joint values led to the successful performance of the task. We recorded the times required to successfully reach the desired positions, number of iterations, and error of the RCM when using the two control methods. The results are presented in Table 1. The task-decoupled method was more robust for different initial

gestures of the supporting arm. Although the proposed method required more iterations than the extended-task method, it achieved a more accurate RCM constraint. Next, the supporting arm was controlled to reach different targets with the same initial joint values. The relative position of the target was set as $[x, y, 30]^\mathrm{T}$. The range of x and y was $[-30, 30]$. Again, 200 random values for x and y were used. In the simulation, four cases with different initial joint values were performed separately using the task-decoupled and extended-task methods. The results are presented in Table 2. According to Table 2, the task-decoupled method could address the majority of the random targets and achieve higher success rates. Therefore, it was more robust allowing the supporting arm to reach different targets with different initial joint values. Furthermore, the proposed method ensured a low error rate for the RCM, less than 0.6 mm. Figure 12 displays the variation of the parameters while reaching a target using the two methods. For the task-decoupled method, the variation in λ was uniform and the RCM error was maintained at a stable low level. This is largely a consequence of the decoupling of the tracking task and RCM constraint. Conflict between the two tasks was avoided.

4.3 Master-Slave Control Evaluation

In this section, we describe the experimental evaluation of the robot in master-slave control mode. The core control algorithm of the robot, written in MATLAB, was integrated into a C++ shared library. The library was then called by a C++ program, which was used to control all the devices including the supporting arm, actuation unit, and master device. In addition, the motion of the robot was visualizable in real time using robotics simulation software (CoppeliaSim). To constrain the motion of the robot, a hysteroscope was inserted into a hole in an acrylic plate. The diameter of the hole was 5 mm and the hole was considered to be the RCM point. The master device was manipulated by an operator. The tip of the robot was controlled to track the desired position

Table 2 Reach random targets with same initial joint values

Method		Success rate	Mean number of iterations	Mean e_{RCM}
Extended task	Case 1	103/200	112	2.04
	Case 2	64/200	189	4.16
	Case 3	0/200	–	–
	Case 4	0/200	–	–
Task decoupled	Case 1	122/200	290	0.56
	Case 2	182/200	216	0.30
	Case 3	154/200	265	0.34
	Case 4	135/200	173	0.42
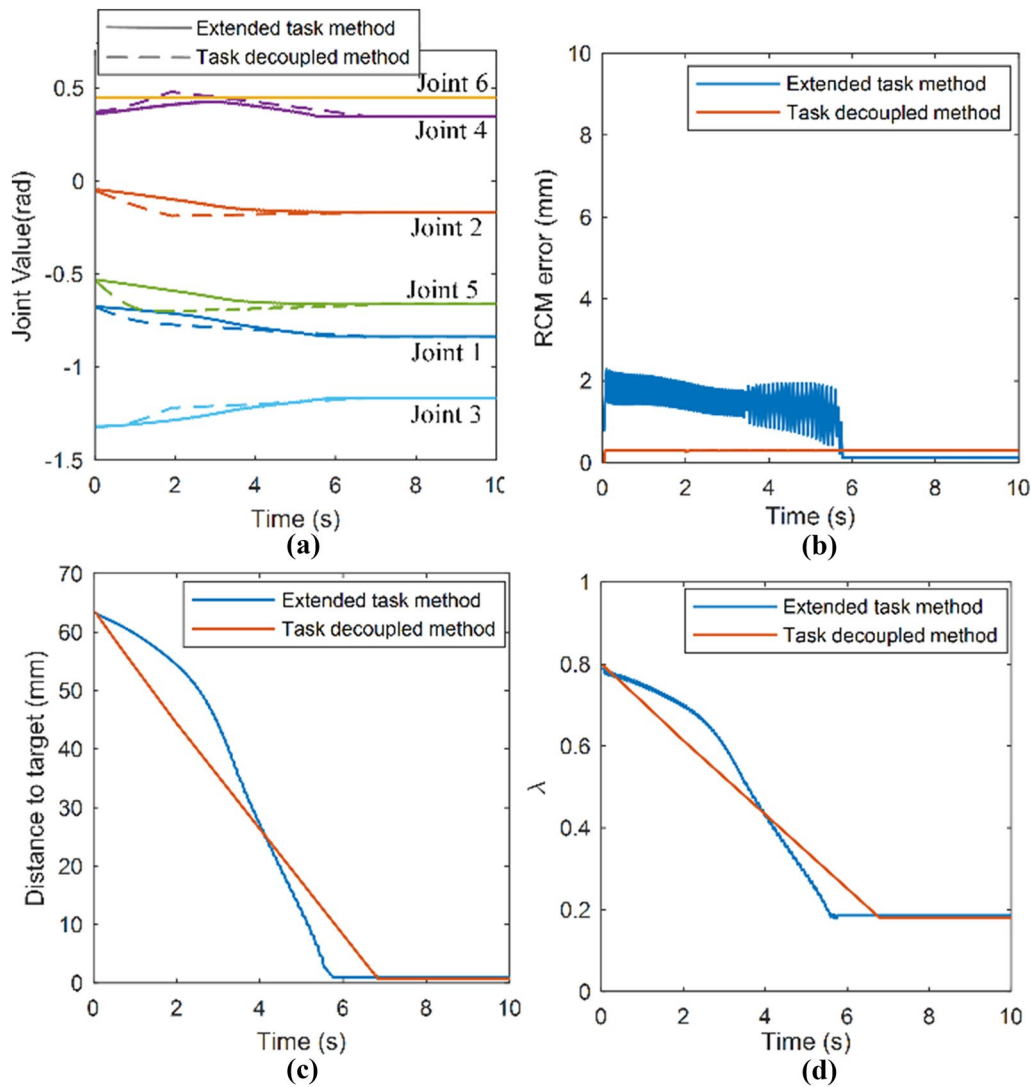
Figure 12 Simulation results for robot to reach target with RCM constraint using two different methods

and direction commanded by the master device at a frequency of 50 Hz. The results of the experiments are presented in Figure 13. The results confirm that the rigid segment of the hysteroscope was well constrained by the RCM point during the entire manipulation process. In addition, the tip of the hysteroscope could reach different positions in different directions because the motion of the robot was constrained by the RCM point.

5 Conclusions

(1) In this paper, we introduced a robotic system with a robust RCM constraint for endometrial regeneration surgery. The robotic system was expected to perform two key processes: processing the endometrium and transplanting stem cells during surgery. To the best of our knowledge, this is the first study of robotic endometrial regeneration surgery.

(2) The robot was composed primarily of a dexterous hysteroscope, actuation unit, and supporting arm. It exhibited high dexterity and compliance. To ensure a valid RCM constraint and predictable hysteroscope shape and posture, the supporting arm and hysteroscope were controlled separately in kinematics. In addition, a novel instrument that could be folded and unfolded was designed to process the endometrium.

(3) To improve the robustness and flexibility of the RCM constraint, we proposed a task-decoupled
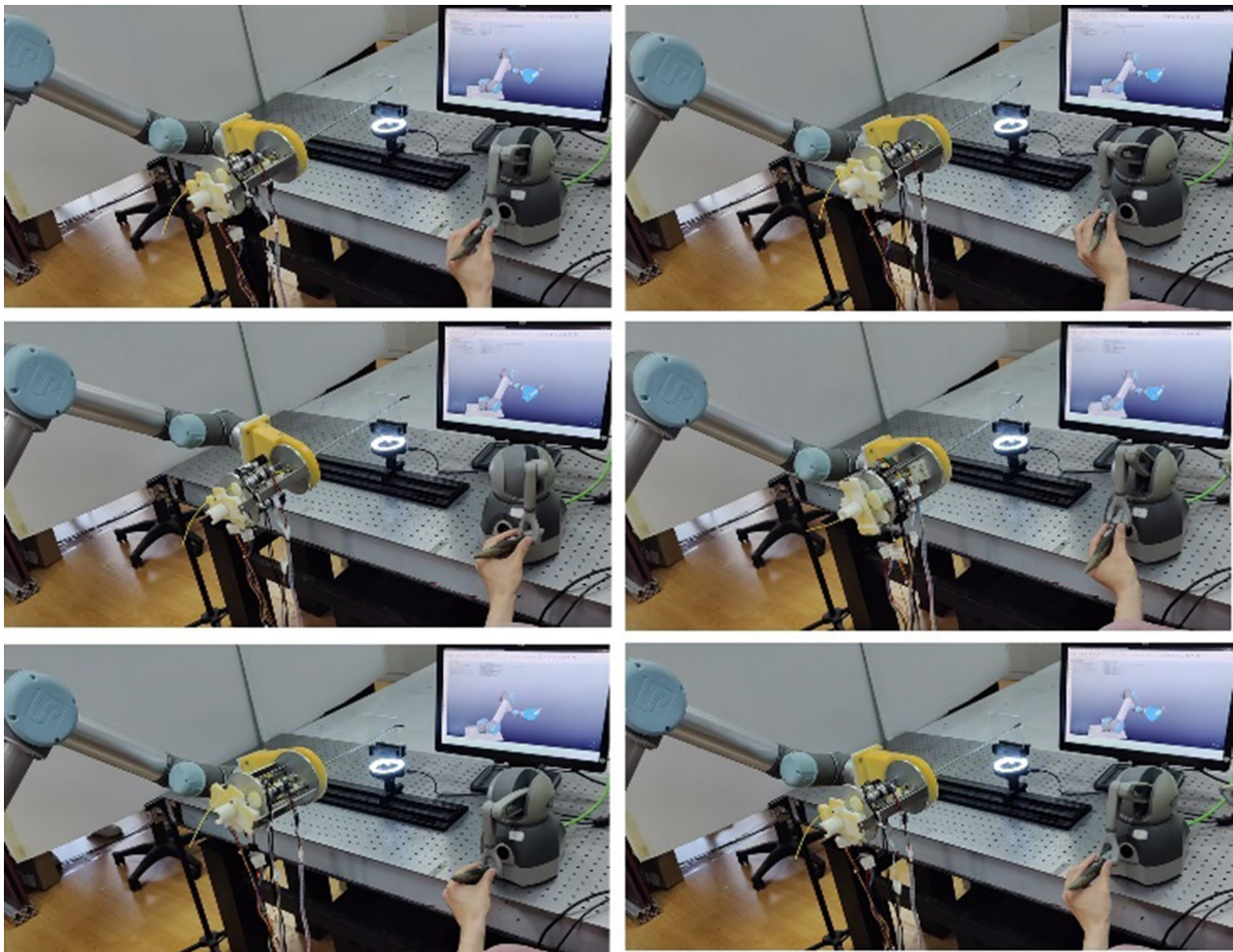
Figure 13 Master-slave control with RCM constraint

method to ensure the RCM constraint. The RCM constraint was considered as the primary task; tip position tracking was realized using the null space of the RCM Jacobian. To avoid conflict between the RCM constraint and tip motion, the motion of the rigid segment of the hysteroscope was decoupled into insertion and directional motion, which were orthogonal to the RCM constraint motion.

(4) Experiments confirmed that the task-decoupled method was more robust than the extended-task method. The task-decoupled method also achieved high RCM accuracy. Lastly, the robot with the RCM constraint was verified under master-slave control.

Authors' Information
Jianhua Li, born in 1992, is currently a PhD candidate at *State Key Laboratory of Robotics, Shenyang Institute of Automation, Chinese Academy of Sciences, and University of Chinese Academy of Science, China*. He received his bachelor degree from *Central South University, China*, in 2016. His research interests include medical robots and systems, continuum robots, and robot control.
Chongyang Wang, born in 1991, is currently a research assistant at *Shenyang Institute of Automation, Chinese Academy of Sciences, China*. He received the B.E. and M.E. degrees from *Harbin Institute of Technology, China*, in 2013 and 2015, respectively. His research interests include surgical robots, medical sensors and robot control.
Zhenxing Wang, born in 1995, is currently a PhD candidate at *Shenyang Institute of Automation, Chinese Academy of Sciences, and University of Chinese Academy of Science, China*. He received his bachelor degree from *Taiyuan University of Technology, China*, in 2018. His research interests include design and control of surgical robotics, continuum robots, and human–robot interaction.
Xiong Zheng, born in 1996, is currently a master degree candidate of *Mechanical Engineering College of Shenyang Jianzhu University, China*. He received his

bachelor degree from *Anhui Jianzhu University, China*, in 2019. His research interests include medical robots and systems, vascular interventional surgery robots and robot control.

Zhidong Wang, born in 1965, is currently a Professor at *Department of Advance Robotics, Chiba Institute of Technology, Japan*. He received the B.S. degree from *Beihang University, China*, in 1987. He received the M.S. and Ph.D. degrees from *Graduate School of Engineering, Tohoku University, Sendai, Japan*, in 1992 and 1995, respectively. His current research interests include human-robot interaction and cooperation systems, distributed autonomous robot systems, micro/nano robotics, and application of intelligent robot technologies for the disabled.

Jichun Tan, born in 1965, is a professor at *Shengjing Hospital of China Medical University, China*. She received the B.S., M.S. and Ph.D. degrees from *Jilin University, China*, in 1986, 1989 and 2003, respectively. Her research interests include infertility, assisted reproductive technology, stem cells, and surgical robot.

Hao Liu, born in 1980, is currently a professor at *Shenyang Institute of Automation, Chinese Academy of Sciences, China*. He received the B.S., M.S., and Ph.D. degrees from the *Harbin Institute of Technology, China*, in 2004, 2006, and 2010, respectively. He worked as a visiting scholar in *Laboratory for Computational Sensing and Robotics, Johns Hopkins University, United States of America* from 2014 to 2015. His research interests include surgical robots, medical sensors, surgical navigation, and robot control.

Competing Interests
The authors declare no competing financial interests.

Author Details
[1]State Key Laboratory of Robotics, Shenyang Institute of Automation, Chinese Academy of Sciences, Shenyang 110016, China. [2]Institutes for Robotics and Intelligent Manufacturing, Chinese Academy of Sciences, Shenyang 110169, China. [3]University of Chinese Academy of Sciences, Beijing 100049, China. [4]Shenyang Jianzhu University, Shenyang 110168, China. [5]Chiba Institute of Technology, Chiba 275-0016, Japan. [6]Shengjing Hospital of China Medical University, Shenyang 110016, China.

References
[1] Meeting to develop a global consensus on preconception care to reduce maternal and childhood mortality and morbidity. *World Health Organization Headquarters,* Geneva, 6-7 February 2012: Meeting report, Geneva Switzerland Who, 2013.
[2] M Vander Borght and C Wyns. Fertility and infertility: definition and epidemiology. *Clinical Biochemistry*, 2018, 62: 2–10.
[3] Z Khan, and J M Goldberg. Hysteroscopic management of asherman's syndrome. *Journal of Minimally Invasive Gynecology*, 2018, 25(2): 218-28.
[4] P Capmas, A Mihalache, L Duminil et al. Intrauterine adhesions: What is the pregnancy rate after hysteroscopic management?. *Journal of Gynecology Obstetrics and Human Reproduction*, 2020, 49(7).
[5] J C Tan, P P Li, Q S Wang et al. Autologous menstrual blood-derived stromal cells transplantation for severe Asherman's syndrome. *Human Reproduction*, 2016, 31(12): 2723-9.
[6] Y T Song, P C Liu, J Tan et al. Stem cell-based therapy for ameliorating intrauterine adhesion and endometrium injury. *Stem Cell Research & Therapy*, 2021, 12(1).
[7] N Gharibeh, L A Maleki, J Madani, et al. Cell-based therapy in thin endometrium and asherman syndrome. *Stem Cell Research & Therapy*, 2022, 13(1).
[8] J B Kahrs, D C Rucker, and H Choset, Continuum robots for medical applications: A survey. *IEEE Transactions on Robotics*, 2015, 31(6): 1261-80.
[9] J Xiao, Y Yang, D Z Li, et al. Advances and key techniques of ophthalmic microsurgical bobots. *Journal of Mechanical Engineering*, 2013: 1. (in Chinese)
[10] N Jang, Y S Ihn, N Choi, et al. Compact and lightweight end-effectors to drive hand-operated surgical instruments for robot-assisted microsurgery. *IEEE/ASME Transactions on Mechatronics*, 2020, 25(4): 1933-43.
[11] Y Chen, C Zhang, Z H Wu, et al. The SHURUI system: a modular continuum surgical robotic platform for multiport, hybrid-port, and single-port procedures. *IEEE/ASME Transactions on Mechatronics*, 2021: 1-12.
[12] L Luko, A Parush, and L Lowenstein, Cognitive task analysis of spatial skills in hysterectomy with the da Vinci surgical system. *IEEE International Conference on Biomedical Engineering (BioMed)*, F, 2017.
[13] L Lowenstein, E Matanes, Z Weiner, et al. Robotic transvaginal natural orifice transluminal endoscopic surgery for bilateral salpingo oophorectomy. *European Journal of Obstetrics & Gynecology and Reproductive Biology*, 2020, 7: 100113.
[14] Y He, B Zhao, X Qi, et al. Automatic surgical field of view control in robot-assisted nasal surgery. *IEEE Robotics and Automation Letters*, 2020, 6(1): 247-54.
[15] E Amanov, D S Ropella, N Nimmagadda, et al. Transurethral anastomosis after transurethral radical prostatectomy: a phantom study on intraluminal suturing with concentric tube robots. *IEEE Transactions on Medical Robotics and Bionics*, 2020, 2(4): 578-81.
[16] R E Goldman, A Bajo, L S MacLachlan, et al. Design and performance evaluation of a minimally invasive telerobotic platform for transurethral surveillance and intervention. *IEEE Transactions on Biomedical Engineering*, 2012, 60(4): 918–25.
[17] A Bajo, L M Dharamsi, J L Netterville, et al. Robotic-assisted micro-surgery of the throat: the trans-nasal approach. *IEEE International Conference on Robotics and Automation*, F, 2013.
[18] J Z Shang, K Leibrandt, P Giataganas, et al. A single-port robotic system for transanal microsurgery—Design and validation. *IEEE Robotics and Automation Letters*, 2017, 2(3): 1510-7.
[19] K C Lau, E Y Y Leung, P W Y Chiu, et al. A flexible surgical robotic system for removal of early-stage gastrointestinal cancers by endoscopic submucosal dissection. *IEEE Transactions on Industrial Informatics*, 2016, 12(6): 2365-74.
[20] C Freschi, V Ferrari, F Melfi, et al. Technical review of the da Vinci surgical telemanipulator. *International Journal of Medical Robotics and Computer Assisted Surgery*, 2013, 9(4): 396-406.
[21] C Y He, L Huang, Y Yang, et al. Research and realization of a master-slave robotic system for retinal vascular bypass surgery. *Chinese Journal of Mechanical Engineering*, 2018, 31(1): 1-10.
[22] C K Kim, D G Chung, M Hwang, et al. Three-degrees-of-freedom passive gravity compensation mechanism applicable to robotic arm with remote center of motion for minimally invasive surgery. *IEEE Robotics and Automation Letters*, 2019, 4(4): 3473-80.
[23] N Aghakhani, M Geravand, N Shahriari, et al. Task control with remote center of motion constraint for minimally invasive robotic surgery. *IEEE International Conference on Robotics and Automation*, F, 2013.
[24] H Sadeghian, F Zokaei, and S Hadian Jazi. Constrained kinematic control in minimally invasive robotic surgery subject to remote center of motion constraint. *Journal of Intelligent & Robotic Systems*, 2018, 95(3–4): 901-13.
[25] H Azimian, R V Patel, and M D Naish. On constrained manipulation in robotics-assisted minimally invasive surgery," in Biomedical Robotics and Biomechatronics (BioRob), *IEEE RAS and EMBS International Conference*, F, 2010.
[26] J Sandoval, G Poisson, and P Vieyres. A new kinematic formulation of the RCM constraint for redundant torque-controlled robots. 2017 *IEEE/RSJ International Conference on Intelligent Robots and Systems (Iros)*, 2017: 4576-81.
[27] J Sandoval, G Poisson, and P Vieyres. Improved dynamic formulation for decoupled cartesian admittance control and RCM constraint. *International Conference on Robotics and Automation (ICRA)*, 2016: 1124-9.
[28] H Su, S Li, J Manivannan, et al. Manipulability optimization control of a serial redundant robot for robot-assisted minimally invasive surgery. *2019 International Conference on Robotics and Automation (Icra)*, 2019: 1323-8.
[29] H Su, C Yang, G Ferrigno, et al. Improved human–robot collaborative control of redundant robot for teleoperated minimally invasive surgery. *IEEE Robotics and Automation Letters*, 2019, 4(2): 1447-53.

[30] X Zhang, W Li, P W Y Chiu, and Z Li. A novel flexible robotic endoscope with constrained tendon-driven continuum mechanism. *IEEE Robotics and Automation Letters*, 2020, 5(2): 1366-72.

[31] W Li, P W Y Chiu, and Z Li. An accelerated finite-time convergent neural network for visual servoing of a flexible surgical endoscope with physical and RCM constraints. *IEEE Transaction on Neural Networks and Learning System*, 2020, 31(12): 5272-84.

[32] J H Li, Y Y Zhou, J C Tan, et al. Design and modeling of a parallel shifted-routing cable-driven continuum manipulator for endometrial regeneration surgery. *IEEE/RSJ International Conference on Intelligent Robots and Systems (IROS)*, F, 2020.

[33] J H Li, Y Y Zhou, C Wang, et al. A model-based method for predicting the shapes of planar single-segment continuum manipulators with consideration of friction and external force. *Journal of Mechanisms and Robotics*, 2020, 12(4): 1-30.